Observation of an optical event horizon in a silicon-on-insulator photonic wire waveguide

Charles Ciret,[1,*] François Leo,[1,2,3] Bart Kuyken,[2,3] Gunther Roelkens,[2,3] and Simon-Pierre Gorza[1]

[1]*OPERA-Photonique, Université libre de Bruxelles (ULB), 50 av. F.D. Roosevelt, CP194/5, B-1050 Bruxelles, Belgium*
[2]*Photonics Research Group, Department of Information Technology, Ghent University-IMEC, Ghent B-9000, Belgium*
[3]*Center for Nano- and Biophotonics (NB-photonics), Ghent University, Ghent B-9000, Belgium*

[*]*charles.ciret@ulb.ac.be*

Abstract: We report on the first experimental observation of an optical analogue of an event horizon in integrated nanophotonic waveguides, through the reflection of a continuous wave on an intense pulse. The experiment is performed in a dispersion-engineered silicon-on-insulator waveguide. In this medium, solitons do not suffer from Raman induced self-frequency shift as in silica fibers, a feature that is interesting for potential applications of optical event horizons. As shown by simulations, this also allows the observation of multiple reflections at the same time on fundamental solitons ejected by soliton fission.

OCIS codes: (190.4380) Nonlinear optics, four-wave mixing; (190.5530) Pulse propagation and temporal solitons; (130.4310) Nonlinear.

References and links

1. R. Dekker, A. Driessen, T. Wahlbrink, C. Moormann, J. Niehusmann, and M. Först, "Ultrafast Kerr-induced all-optical wavelength conversion in silicon waveguides using 1.55 μm femtosecond pulses," Opt. Express **14**, 8336–8346 (2006).
2. I-W. Hsieh, X. Chen, J. I. Dadap, N. C. Panoiu, R. M. Osgood, Jr., S. J. McNab, and Y. A. Vlasov, "Cross-phase modulation-induced spectral and temporal effects on co-propagating femtosecond pulses in silicon photonic wires," Opt. Express **15**, 1135–1146 (2007).
3. Q. Lin, O. J. Painter, and G. P. Agrawal, "Nonlinear optical phenomena in silicon waveguides: modeling and applications," Opt. Express **15**, 16604–16644 (2007).
4. G. P. Agrawal, *Nonlinear Fiber Optics*, 5th ed. (Academic Press, 2012).
5. D. Dimitropoulos, V. Raghunathan, R. Claps, and B. Jalali, "Phase-matching and nonlinear optical processes in silicon waveguides," Opt. Express **12**, 149–160 (2004).
6. J. E. Sharping, K. F. Lee, M. A. Foster, A. C. Turner, B. S. Schmidt, M. Lipson, A. L. Gaeta, and P. Kumar, "Generation of correlated photons in nanoscale silicon waveguides," Opt. Express **14**, 12388–12393 (2004).
7. J. Hansryd, P.A. Andrekson, M. Westlund, L. J. Li, and P. Hedekvist, "Fiber-based optical parametric amplifiers and their applications," IEEE J. Sel. Top. Quantum Electron. **8**, 506–520 (2002).
8. T. G. Philbin, C. Kuklewicz, S. Robertson, S. Hill, F. König, and U. Leonhardt, "Fiber-optical analog of the event horizon," Science **319**, 1367–1370 (2008).
9. T. G. Philbin, C. Kuklewicz, S. Robertson, S. Hill, F. König, and U. Leonhardt, "Fiber-optical analogue of the event horizon: Appendices," arXiv:0711.4796 (2008).
10. D. Faccio, T. Arane, M. Lamperti, and U. Leonhardt, "Optical black hole lasers," Classical and Quantum Gravity **29**, 224009 (2012).

#253529 Received 6 Nov 2015; revised 19 Dec 2015; accepted 22 Dec 2015; published 5 Jan 2016

11. K. E. Webb, M. Erkintalo, Y. Xu, N. G. R. Broderick, J. M. Dudley, G. Genty, and S. G. Murdoch, "Nonlinear optics of fibre event horizons," Nat Commun **5** (2014).
12. Y. Q. Xu, M. Erkintalo, G. Genty, and S. G. Murdoch, "Cascaded bragg scattering in fiber optics," Opt. Lett. **38**, 142–144 (2013).
13. A. V. Yulin, D. V. Skryabin, and P. S. J. Russell, "Four-wave mixing of linear waves and solitons in fibers with higher-order dispersion," Opt. Lett. **29**, 2411–2413 (2004).
14. D. V. Skryabin and A. V. Yulin, "Theory of generation of new frequencies by mixing of solitons and dispersive waves in optical fibers," Phys. Rev. E **72**, 016619 (2005).
15. A. Efimov, A. Taylor, F. Omenetto, A. Yulin, N. Joly, F. Biancalana, D. Skryabin, J. Knight, and P. Russell, "Time-spectrally-resolved ultrafast nonlinear dynamics in small-core photonic crystal fibers: Experiment and modelling," Opt. Express **12**, 6498–6507 (2004).
16. A. Efimov, A. V. Yulin, D. V. Skryabin, J. C. Knight, N. Joly, F. G. Omenetto, A. J. Taylor, and P. Russell, "Interaction of an optical soliton with a dispersive wave," Phys. Rev. Lett. **95**, 213902 (2005).
17. A. Choudhary and F. König, "Efficient frequency shifting of dispersive waves at solitons," Opt. Express **20**, 5538–5546 (2012).
18. L. Tartara, "Frequency shifting of femtosecond pulses by reflection at solitons," IEEE J. Quantum Electron. **48**, 1439–1442 (2012).
19. A. Bendahmane, A. Mussot, M. Conforti, and A. Kudlinski, "Observation of the stepwise blue shift of a dispersive wave preceding its trapping by a soliton," Opt. Express **23**, 16595–16601 (2015).
20. S. F. Wang, A. Mussot, M. Conforti, A. Bendahmane, X. L. Zeng, and A. Kudlinski, "Optical event horizons from the collision of a soliton and its own dispersive wave," Phys. Rev. A **92**, 023837 (2015).
21. I. Oreshnikov, R. Driben, and A. V. Yulin, "Weak and strong interactions between dark solitons and dispersive waves," Opt. Lett. **40**, 4871–4874 (2015).
22. A. V. Yulin, R. Driben, B. A. Malomed, and D. V. Skryabin, "Soliton interaction mediated by cascaded four wave mixing with dispersive waves," Opt. Express **21**, 14481–14486 (2013).
23. S. F. Wang, A. Mussot, M. Conforti, X. L. Zeng, and A. Kudlinski, "Bouncing of a dispersive wave in a solitonic cage," Opt. Lett. **40**, 3320–3323 (2015).
24. R. Driben, F. Mitschke and N. Zhavoronkov, "Cascaded interactions between Raman induced solitons and dispersive waves in photonic crystal fibers at the advanced stage of supercontinuum generation," Opt. Express **18**, 25993–25998 (2010).
25. R. Driben, A. V. Yulin, A. Efimov, and B. A. Malomed, "Trapping of light in solitonic cavities and its role in the supercontinuum generation," Opt. Express **21**, 19091–19096 (2013).
26. A. Demircan, S. Amiranashvili, C. Brée, and G. Steinmeyer, "Compressible octave spanning supercontinuum generation by two-pulse collisions," Phys. Rev. Lett. **110**, 233901 (2013).
27. S. M. Hawking, "Black holes explosions?" Nature **248**, 30 (1974).
28. J. M. Dudley, G. Genty, and S. Coen, "Supercontinuum generation in photonic crystal fiber," Rev. Mod. Phys. **78**, 1135–1184 (2006).
29. A. Demircan, S. Amiranashvili, and G. Steinmeyer, "Controlling light by light with an optical event horizon," Phys. Rev. Lett. **106**, 163901 (2011).
30. L. Tartara, "Soliton control by a weak dispersive pulse," J. Opt. Soc. Am. B **32**, 395–399 (2015).
31. L. Zhang, Q. Lin, Y. Yue, Y. Yan, R. Beausoleil, A. Agarwal, L. Kimerling, J. Michel, and A. Willner, "On-chip octave-spanning supercontinuum in nanostructured silicon waveguides using ultralow pulse energy," IEEE J. Sel. Top. Quantum Electron. **18**, 1799–1806 (2012).
32. R. Halir, Y. Okawachi, J. S. Levy, M. A. Foster, M. Lipson, and A. L. Gaeta, "Ultrabroadband supercontinuum generation in a CMOS-compatible platform," Opt. Lett. **37**, 1685–1687 (2012).
33. F. Leo, S.-P. Gorza, J. Safioui, P. Kockaert, S. Coen, U. Dave, B. Kuyken, and G. Roelkens, "Dispersive wave emission and supercontinuum generation in a silicon wire waveguide pumped around the 1550 nm telecommunication wavelength," Opt. Lett. **39**, 3623–3626 (2014).
34. U. D. Dave, C. Ciret, S.-P. Gorza, S. Combrie, A. De Rossi, F. Raineri, G. Roelkens, and B. Kuyken, "Dispersive-wave-based octave-spanning supercontinuum generation in InGaP membrane waveguides on a silicon substrate," Opt. Lett. **40**, 3584–3587 (2015).
35. J. P. Gordon, "Theory of the soliton self-frequency shift," Opt. Lett. **11**, 662–664 (1986).
36. N. Singh, D. D. Hudson, Y. Yu, C. Grillet, S. D. Jackson, A. Casas-Bedoya, A. Read, P. Atanackovic, S. G. Duvall, S. Palomba, B. Luther-Davies, S. Madden, D. J. Moss, and B. J. Eggleton, "Midinfrared supercontinuum generation from 2 to 6 μm in a silicon nanowire," Optica **2**, 797–802 (2015).
37. R. A. Soref and B. R. Bennett, "Electrooptical effects in silicon," IEEE J. Quantum Electron. **23**, 123–129 (1987).
38. R. Claps, D. Dimitropoulos, V. Raghunathan, Y. Han, and B. Jalali, "Observation of stimulated Raman amplification in silicon waveguides," Opt. Express **11**, 1731–1739 (2003).
39. L. Yin, Q. Lin, and G. P. Agrawal, "Soliton fission and supercontinuum generation in silicon waveguides," Opt. Lett. **32**, 391–393 (2007).
40. N. Akhmediev and M. Karlsson, "Cherenkov radiation emitted by solitons in optical fibers," Phys. Rev. A. **51**,

#253529 Received 6 Nov 2015; revised 19 Dec 2015; accepted 22 Dec 2015; published 5 Jan 2016

2602–2607 (1995).
41. D. V. Skryabin and A. V. Gorbach, "*Colloquium* : Looking at a soliton through the prism of optical supercontinuum," Rev. Mod. Phys. **82**, 1287–1299 (2010).
42. S. Robertson and U. Leonhardt, "Frequency shifting at fiber-optical event horizons: The effect of Raman deceleration," Phys. Rev. A. **81**, 063835 (2010).
43. D. A. B. Miller, "Are optical transistors the logical next step?" Nat. Photon. **4**, 3–5 (2010).

1. Introduction

The nonlinear interactions between optical waves in Kerr media have attracted a lot of attention in the scientific community for many years. Among others, we can cite studies involving cross-phase modulation (XPM) effects [1–4], or four wave mixing processes [3–7]. Recently, it has been shown that some of these interactions can mimic, under some circumstances, the interactions occurring at the horizons of black and white holes [8–11]. These so-called optical event horizons occur when an intense pulse, propagating in a nonlinear waveguide, prevents a weak probe wave traveling at a different velocity from passing through it. The intense pulse induces a moving refractive index perturbation which in turn leads to a frequency conversion of the probe through a cross-phase modulation effect. Since this interaction take place in a dispersive medium, the frequency conversion of the probe in the spectral domain alters the velocity of the probe that is either accelerated or decelerated, preventing any crossing between the two waves. The intense pulse thus constitutes an horizon which light can neither join nor escape. More recently, it has also been shown that this frequency conversion can be modeled through a cascaded four wave mixing mechanism [11, 12]. The frequency conversion was first theoretically predicted by Yulin *et al.* [13, 14], well before the analogy with the event horizons was established, and experimentally observed in the meantime in the context of supercontinuum generation (SCG) in optical fibers [15, 16]. Since then numerous experimental demonstrations have been realized in optical fibers, by superimposing at the fiber input a weak probe wave together with an intense pulse [8, 11, 17], by the interaction of two pulses [18] or by the collision between an intense pulse and its own dispersive waves generated in topographic fibers designed for that purpose [19, 20]. Recent theoretical studies have also investigated the interactions between dark solitons and dipersive waves [21] or the trapping of dispersive waves between two optical solitons which undergo multiple reflections between them [22]. The latter has also been demonstrated experimentally [23], and its role in the SCG has been theoretically studied [24–26].

The optical event horizons have been widely studied for their analogies with the general relativity in that sense that they could act as a laboratory scale universe, to research effects such as the Hawking radiation [8, 9, 27]. They have also attracted a lot of attention for practical applications. In this way, this phenomenon has been pointed out as an efficient mechanism to convert the frequency of a signal [18] in a complementary manner from the interactions involving the emission of a Cherenkov radiation, also known as dispersive wave (DW). The latter has been extensively studied in the context of SCG and constitute also an efficient way for the transfer of energy far from the intense pulse wavelength [28]. Moreover, the strong light-light interaction arising at an optical event horizon could lead to a spectral recoil of the pump, a mechanism that has been recognized as suitable for the future demonstration of all-optical transistor functionalities [29, 30], by fulfilling all the mandatory arduous criteria in particular fan-out and cascadability, which are the most difficult to meet.

In this paper, we report on the first experimental demonstration of an optical event horizon in a fully CMOS-compatible integrated nanophotonic waveguide by the interaction of a weak continuous probe wave (CW probe) with a strong pump pulse. Such platforms have already been successfully used, among others, for the generation of supercontinuum at telecommunication wavelengths [31–33]. The dispersion properties of the structure, essential to the observation of

#253529 Received 6 Nov 2015; revised 19 Dec 2015; accepted 22 Dec 2015; published 5 Jan 2016

optical event horizons, have been tailored through the waveguide dimensions. We show that, thanks to the inherent high confinement in these structures, resulting in strong nonlinearities, the interaction takes place on millimeter length scales using picojoule pump pulses. The total length and the input pulse energy needed are therefore three orders of magnitude lower than those required for the previous experiments performed in optical fibers, for which meter scale propagation and nanojoule input pulses were needed. The experimental results are unambiguously confirmed by numerical simulations using the generalized nonlinear Schrödinger equation (GNLSE) taking into account the specific nonlinear phenomena involved in nanophotonic silicon waveguides, namely the role of the free-carriers, the effect of the two-photon absorption and the narrow Raman gain spectrum. The absence of the Raman induced self-frequency shift of solitons in silicon waveguides is a major difference with silica fibers. As shown in this work, this enables multiple reflections at the same time of a probe wave on solitons generated by soliton fission. Moreover, regarding potential applications of optical event horizons, this absence is beneficial as it has a strong influence on the soliton group velocity [29]. Finally, from numerical simulations, we show that, a quasi-complete conversion of the probe as well as a non negligible spectral recoil of the pump could in principle be achieved for two pulses interactions, making these structures very good candidates for the realization of integrated low power all-optical functionalities in a low-cost, high volume fabrication platform.

2. Model

Let consider a CW probe at ω_{probe} propagating with an intense pulsed pump at ω_{pump} in a nonlinear dispersive waveguide. In such a situation, it has been shown that the nonlinear interaction between the two waves can be interpreted as a cascaded-four wave mixing mechanism, leading to a frequency conversion of the CW probe [11]. The conversion from the probe wavelength to a single higher-order idler wavelength component ω_{idler} is efficient when the resonant condition [11, 12]:

$$D(\omega_{idler} - \omega_{pump}) = D(\omega_{probe} - \omega_{pump}), \tag{1}$$

is fulfilled. The wavenumber $D(\omega - \omega_{pump}) = \beta(\omega) - \beta_0 - \beta_1 \times (\omega - \omega_{pump})$ [where $\beta_0 = \beta(\omega_{pump})$ and $\beta_1 = d\beta/d\omega|_{\omega_{pump}}$] is the wavenumber of a linear wave at a frequency ω in a reference frame co-moving with the pump pulse at a frequency ω_{pump}. In the temporal domain, this frequency shift is the result of the nonlinear phase imprinted upon the CW wave by the pump pulse.

The evolution of the wavenumber D as a function of wavelength for different pump wavelengths is displayed in Fig. 1 for the waveguide used in the experiment. Considering a CW probe at 1541 nm (see dashed line as well as the P point on the blue curve), we can infer from this figure that the idler wave satisfying the resonance condition Eq. (1) (see the I point for the blue curve) is located on the other side of the minimum of the wavenumber D versus wavelength curve (VM point for the blue curve). This peculiar VM position corresponds to the wavelength that is group velocity matched with the pump wave. For a 2165 nm pump (blue curve), the CW probe at 1541 nm travels faster than the pump and the change in the group velocity resulting from the frequency shift prevents the CW wave to cross the pump pulse. The trailing edge of the pump pulse thus corresponds to an optical horizon for the probe, similar to a white-hole horizon. The same reasoning can be made for a probe wave traveling slower than the pump. In this case the leading edge of the pump is similar to a black-hole horizon. The linear dispersion properties of the structure thus plays an essential role for the observation of an optical event horizon, and particularly the variation of the group velocity in the vicinity of the VM point. This could explain that all the previous experimental demonstrations have been realized in optical fibers, for which nearly on-demand dispersion properties can be engineered, particularly

#253529 Received 6 Nov 2015; revised 19 Dec 2015; accepted 22 Dec 2015; published 5 Jan 2016

since the advent of the photonic crystal fibers. However, in silica fibers, the broad Raman gain should be taking into account through a continuous modification of the phase-matching condition along the propagation distance [9], as it leads to the continuous redshift of the pump and hence to the corresponding blueshift of the VM point. On the contrary, in silicon waveguides the wavelength of the VM point does not change since the peaked Raman gain prevents the soliton self-frequency shift.

3. Experimental demonstration and numerical simulations

Our demonstration is realized in a 22 mm-long silicon-on-insulator waveguide with a height of 220 nm and a width of 880 nm. The dimensions of the waveguide have been carefully chosen in order to tailor its linear dispersion properties, according to the conditions to observe an optical event horizon as discussed above. The waveguide has two zero-dispersion wavelengths at 1740 nm and at 2390 nm, respectively (see in the inset in Fig. 1). The first zero dispersion wavelength is located between the probe wavelength in the telecom C-band and the pump wavelength which is in the anomalous dispersion regime. The intense pump pulse at a wavelength of 2085 nm is generated by an optical parametric oscillator (OPO, Spectra Physics OPAL) delivering 180 fs pulses (full width at half maximum, FWHM) at 82 MHz repetition rate. The CW probe, for which the wavelength can be tuned from 1538 nm to 1545 nm, is generated by a CW laser followed by an Er-doped fiber amplifier. At the amplifier output, the CW beam is collimated and the two beams are combined by means of a dichroic mirror. The beams are then coupled into the photonic nanowire using a microscope objective, each of them exciting only the quasi-TE mode of the waveguide. At the waveguide output, the light is collected by a lensed fiber and sent to an optical spectrum analyzer (OSA). The experimental output spectra recorded in the range 1250 nm-1700 nm, i.e. up to the wavelength cut-off of our OSA, are displayed in Fig. 2(a) for an on-chip peak pump power of 6.5 W and a 500 μW CW probe. In the experiment, the pump power was progressively increased until the emergence of an idler wave,

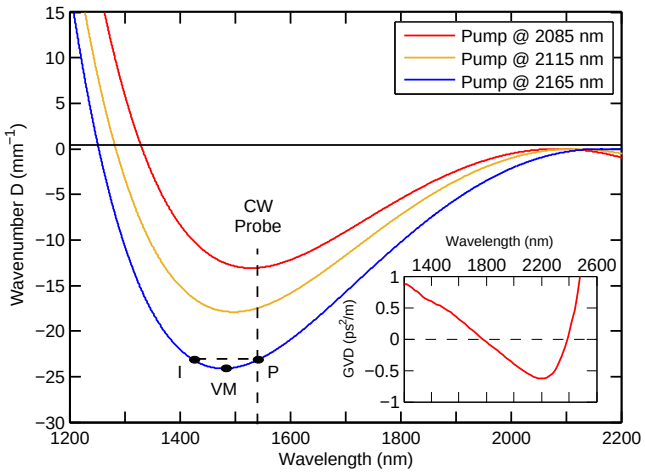

Fig. 1. Wavenumber D as a function of the wavelength for different pump wavelengths. The vertical dashed line represents the position of the continuous probe wave at 1541 nm. The GVD curve for our 220 nm-thick, 880 nm-wide silicon nanophotonic waveguide is shown in the inset. GVD: group velocity dispersion, CW: continuous wave. P, I and VM points, see discussion in the text (indicated only for the blue curve for clarity).

#253529 Received 6 Nov 2015; revised 19 Dec 2015; accepted 22 Dec 2015; published 5 Jan 2016

signature of the reflection of the probe onto the pump, was clearly visible in the spectrum. The corresponding simulations are shown in Fig. 2(b). They were performed by solving the GNLSE with a split-step Fourier algorithm. The GNLSE describes the temporal evolution of the complex envelope of the electric field $A(z,t)$. It was successfully used to simulate SC generation in nanophotonic waveguides, involving spectra spanning more than one octave [34], and even up to 4000 nm [36]. It reads [28]:

$$\frac{\partial A(z,t)}{\partial z} = i\sum_{k=2}^{\infty}\frac{i^k}{k!}\beta_k\frac{\partial^k A(z,t)}{\partial t^k} - \frac{\alpha_0}{2}A(z,t) - \frac{\alpha_c}{2}(1+i\mu)A(z,t) + i\gamma(1+i\tau_{\text{shock}}\frac{\partial}{\partial t})A(z,t)\int_{-\infty}^{+\infty}R(t')\left|A(z,t-t')\right|^2 dt'. \quad (2)$$

In this equation, $\beta_k = \partial^k\beta/\partial\omega^k$ are the dispersion coefficients associated with the Taylor series expansion of the propagation constant $\beta(\omega)$ around the pump frequency ω_{pump}. The corresponding terms in the equation describe the linear dispersion effect. However in the simulations, as recommended by [28], the dispersion operator is directly applied without approximation in the frequency domain, from the function $\beta(\omega)$. This latter function has been computed by finite difference on the whole wavelength range of interest. $\alpha_0 = 2\text{dB/cm}$ is the linear loss coefficient, $\alpha_c = \sigma N_c$ accounts for the free-carrier absorption losses, where N_c is the free-carrier density and $\sigma = 1.45\times10^{-21}$ m^2 for silicon [3], $\mu = 2k_c\omega_{pump}/(\sigma c)$ is the free-carrier dispersion where c is the speed of light and $k_c = (8.8\times10^{-28}N_c + 1.35\times10^{-22}N_c^{0.8})/N_c$ is the free-carrier index [3, 37]. $\gamma = (234+i15)$ W^{-1}m^{-1} is the complex nonlinear parameter and $R(t')$ is the response function accounting for the instantaneous and delayed Raman contributions to the nonlinearity [3, 33, 38]. The dispersion of the nonlinearity is modeled by the time derivative term in the nonlinear terms, where $\tau_{\text{shock}} = 1/\omega_{pump} + 1/n_2\partial n_2/\partial\omega - 1/a_{eff}\partial a_{eff}/\partial\omega$, with n_2 the Kerr nonlinear coefficient and a_{eff} the effective mode area. In this work, we have approximated τ_{shock} to $1/\omega_{pump}$ as in [33].

Finally, the GNLSE is coupled to the equation that describes the dynamics of the carrier density:

$$\frac{\partial N_c(z,t)}{\partial t} = \frac{2\pi\text{Im}(\gamma)}{h\omega_{pump}a_{eff}}|A(z,t)|^4 - \frac{N_c(z,t)}{\tau_c}, \quad (3)$$

where $\tau_c = 1$ ns is the carrier lifetime and h is the Planck's constant. As seen in Figure 2, a very good agreement is achieved between the experimental results and the simulations despite the strong approximation related to the dispersion of the nonlinear coefficient.

At the pump power needed to observe the reflection of the probe, it can be seen in Fig. 2 (black curves) and Figs. 3(a) and 3(b) and in Fig. 4, that the pump pulse propagation in the anomalous dispersion region leads to the generation of a supercontinuum. As shown previously, the spectral broadening is the result of self-phase modulation (SPM), soliton splitting, as well as the emission of DWs [33, 39]. DWs are generated in the normal dispersion region, around 1330 nm and 2768 nm (this latter DW is not seen on the experimental spectra as it is outside the wavelength range of our optical spectrum analyzers). These wavelengths satisfy the phase matching condition [40]: $\beta(\omega_{DW}) - \omega_{DW}/v_{g,pump} = \beta(\omega_{pump}) - \omega_{pump}/v_{g,pump} + \gamma P_{pump}/2$, where ω_{DW} is the frequency of the DW, P_{pump} and $v_{g,pump}$ are the pump peak power and group velocity, respectively. For the DW around 1330 nm, this peculiar wavelength corresponds to the crossing point between the D curves and the horizontal black line in Fig. 1. When only the pump pulse is coupled in the waveguide, only the DW is visible below 1700 nm in the recorded output spectrum as shown in Fig. 2(a). The output spectrum of the CW alone is shown as the gray curves in Fig. 2.

#253529 Received 6 Nov 2015; revised 19 Dec 2015; accepted 22 Dec 2015; published 5 Jan 2016

When both the pump and the CW probe are propagating together, the output spectra show other distinctive features. Close to the probe wavelength a wide pedestal can be seen. It is generated during the first part of the propagation dynamics [see Fig. 3(c)] and is the result of the cross phase modulation on the CW probe which overlaps with the input pump pulse. On either sides of the probe, two narrow peaks, labeled RS and RAS in Fig. 2, can also be identified.

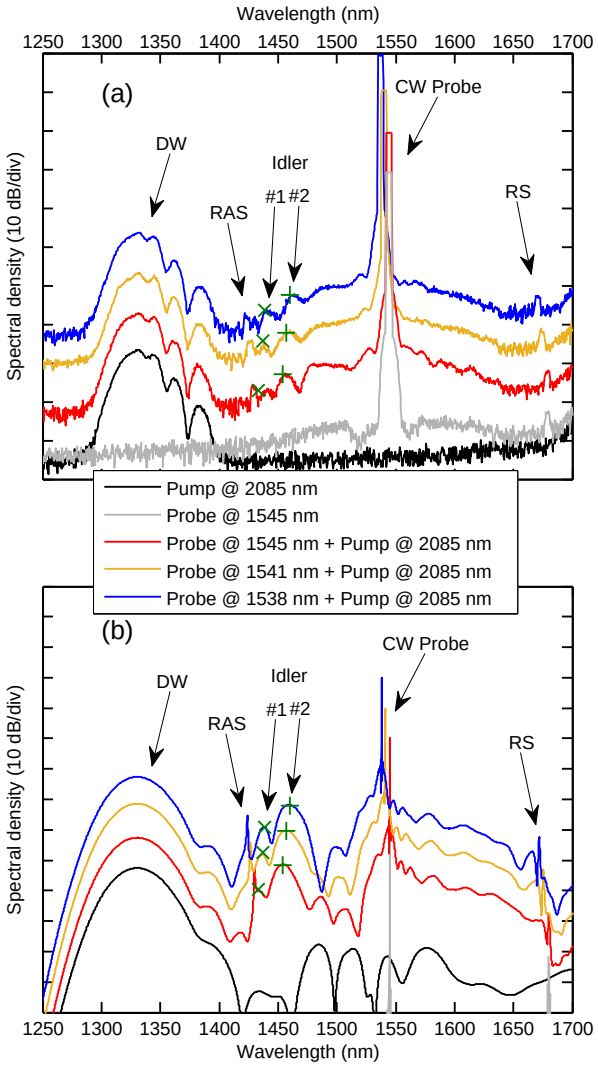

Fig. 2. Experimental spectra recorded at the output of our 22 mm-long Si waveguide (a) and the corresponding simulated spectra (b) for a 6.5 W, 180 fs $sech^2$-shaped input pump wave at 2085 nm. These curves show the output spectra with the pump alone (black curves), with only the 500 μW CW probe at 1545 nm (gray curves), and with both the pump and the CW probe at different wavelengths (other colors). The arrows labeled Idler #1 and #2 show two reflected waves that are shifted when the probe wavelength is tuned. The curves are shifted by 10 dB for clarity, except for the gray and the black curves. Markers : see discussion in the text. DW: dispersive wave, CW: probe wave, RAS: Raman anti-Stokes, RS: Raman Stokes.

#253529 Received 6 Nov 2015; revised 19 Dec 2015; accepted 22 Dec 2015; published 5 Jan 2016

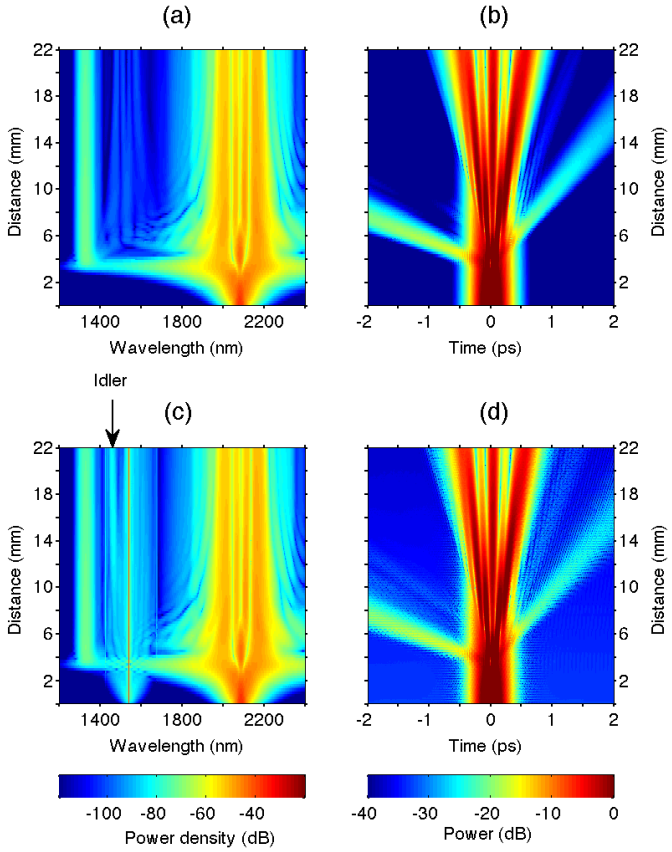

Fig. 3. Pseudocolor plots of the simulated spectral [(a), (c)] and temporal [(b), (d)] evolution along the 22 mm propagation for a 6.5 W, 180 fs $sech^2$-shaped input pump wave at 2085 nm propagating without [(a), (b)] and with the 500 μW CW probe at 1541 nm [(c), (d)]. The arrow highlights the frequency conversion of the CW probe toward the two idler waves at 1457 nm and 1436 nm. Note that in this figure the two idler waves are not spectrally resolved.

These peaks are ±17 THz away from the wavelength of the CW probe and correspond to the generation of Raman anti-Stokes (RAS) and Raman Stokes (RS) photons from the probe wave, as confirmed by canceling in the simulation the delayed nonlinear term in Eq. (2). They come from the amplification of both the noise and the photons resulting from the spectral broadening of the pump pulse and the CW wave spectra by SPM and XPM. The remaining features are the two broad peaks labeled Idler #1 and #2. Their positions agree quite well with the numerical simulations and are clearly shifted toward the probe for decreasing probe wavelength. The simulated spectral and temporal evolution along the propagation distance plotted in Fig. 3(c) and 3(d) show that the reflection of the CW probe actually occurs after the soliton fission that follows the temporal pulse compression. [Note that the reflection of the probe onto the pump is not clearly visible in the simulated temporal evolution plotted in Fig. 3(d) because the probe is a continuous wave giving an almost temporal uniform background.] The fundamental solitons resulting from the fission have a pulse duration of 70 fs and are centered around 2115 nm, 2165 nm and 1995 nm. The simulations displayed in Fig. 4 with an input pulse corresponding

#253529 Received 6 Nov 2015; revised 19 Dec 2015; accepted 22 Dec 2015; published 5 Jan 2016

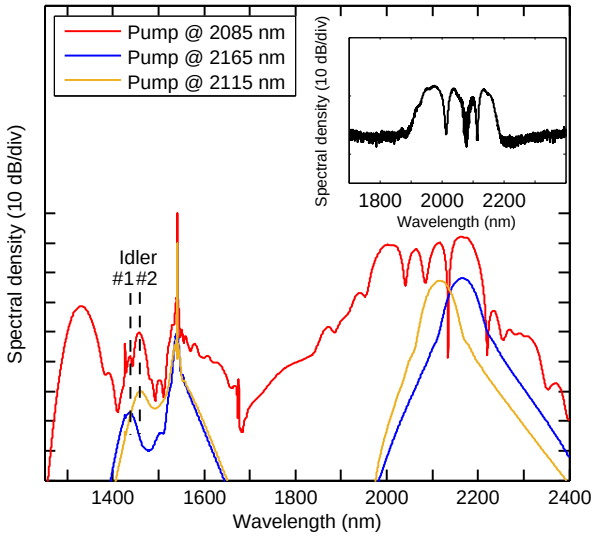

Fig. 4. Simulated output spectra for a 500 µW CW input probe at 1541 nm together with a 6.5 W, 180 fs $sech^2$-shaped input pump wave at 2085 nm (red curve) or with a 1.8 W, 70 fs $sech^2$-shaped input pump wave at 2115 nm (yellow curve) or at 2165 nm (blue curve). The corresponding output spectrum, recorded with a Fourier transform optical spectrum analyser, for a 6.5 W, 180 fs input pump wave at 2085 nm is shown in the inset in the wavelength range 1700 nm-2400 nm. The red curve is shifted by 10 dB for clarity. Note that the RS and RAS peaks are barely visible for low pump peak power because of the reduced spectral broadening of the pump and the probe.

to one of these fundamental solitons with the same peak power as just after the fission (1.8 W) clearly show that, in our experiment, the Idler #1 wave is the result of the reflection of the probe on the soliton emitted at 2165 nm and the Idler #2 is related to the reflection on the soliton at 2115 nm. Moreover, we have verified that the idler wavelength depends on the probe wavelength. We can observe in Fig. 2 (both in the experimental and the numerical spectra) that when the CW probe is shifted toward the zero slope wavelength (VM point), the idler wavelength also gets closer to that wavelength, as shown in Fig. 1. The generated Idler wavelengths #1 and #2 are in excellent agreement with the theoretical wavelengths predicted by the resonant condition Eq. (1), considering a soliton at 2165 nm and at 2115 nm, respectively. These theoretical wavelengths are depicted in Fig. 2(a) and 2(b) by the ($\times$) and ($+$) markers respectively. This confirms the central role played by the resonant condition on the wavenumber D as seen in the previous demonstrations of optical event horizons in optical fibers [11]. The observation of two reflections at the same time is mainly due to the absence of a broad Raman gain band close to the pump wavelength, which prevents the soliton self-frequency shift effect. Consequently, the solitons generated after the fission process remain very close to each other in the spectral domain and consequently also in the time domain, as it can be seen in Fig. 3(a)-3(d). Therefore, their corresponding group velocity matched wavelengths are almost identical which is a crucial point to observe multiple reflections at the same time. Indeed, as previously shown [8, 9], the CW probe wave can be wavelength-shifted over a limited range around the VM point, according to:

#253529 Received 6 Nov 2015; revised 19 Dec 2015; accepted 22 Dec 2015; published 5 Jan 2016

$$\delta\lambda = \frac{\sqrt{4\lambda_{VM}\lambda_0}}{T_0\omega_{VM}}\sqrt{\left|\frac{\beta_2(\lambda_0)}{\beta_2(\lambda_{VM})}\right|}, \tag{4}$$

where λ_0 and λ_{VM} correspond, respectively to the wavelength of the considered soliton and the corresponding VM point, T_0 is the soliton pulse duration, $\beta_2(\lambda_0)$ and $\beta_2(\lambda_{VM})$ are respectively, the second order dispersion coefficients computed at the soliton wavelength and at the corresponding VM point. Beyond this bandwidth, the efficiency of the conversion falls rapidly. The suitable wavelength range in our experiment is thus ± 50 nm around the VM point corresponding to each soliton. The probe wavelengths are 40 ± 5 nm away from the VM point for the solitons at 2115 nm and are 50 ± 5 nm away from the VM points for both the solitons at 2165 nm and at 1995 nm, i.e. at the limit of the bandwidth. This could explain that the Idler #1 are less pronounced than the Idler #2. Moreover, as we use a CW probe, only a small part of the total probe light is converted during the propagation, according to [9, 18]:

$$\eta = \frac{L}{c}\nu_{rep}\left|\Delta n_g\right| \tag{5}$$

where, L is the total interaction length, ν_{rep} is the repetition rate of the pump pulse train and Δn_g is the difference of the group indices between the pump and the CW probe. The theoretical conversion efficiency which is around -45 dB for the reflection on the solitons at 2115 nm and at 2165 nm, is 5 dB weaker for the reflection on the soliton at 1995 nm. This, together with the fact that the signal is close to the conversion bandwidth limit for the soliton at 1995 nm, explain that the Idler #3 cannot emerge from the wide pedestal of the probe. Similarly, even though a sufficient refractive index change for the observation of an event horizon may be reached when

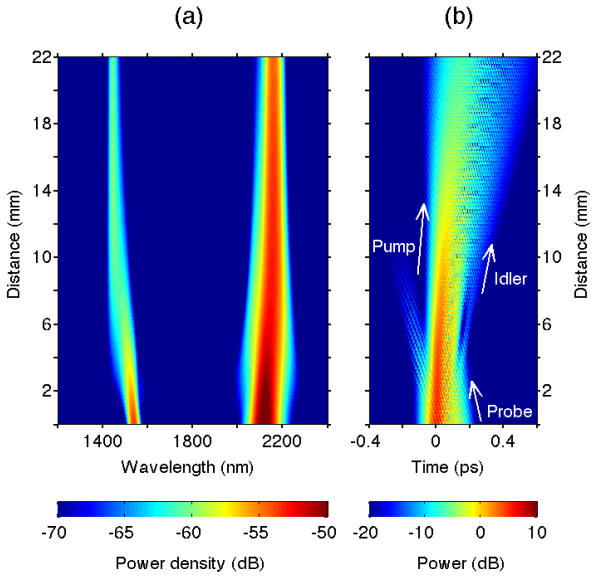

Fig. 5. Pseudocolor plots of the simulated spectral (a) and temporal (b) evolutions along the 22 mm propagation for a 3 W, 70 fs $sech^2$-shaped input pump wave at 2115 nm propagating with a 500 mW, 180 fs $sech^2$-shaped input probe at 1541 nm delayed by 100 fs with respect to the pump. A nearly complete frequency conversion of the probe and a spectral recoil of the pump are observed as well as the temporal reflection of the probe into the pump.

#253529 Received 6 Nov 2015; revised 19 Dec 2015; accepted 22 Dec 2015; published 5 Jan 2016

the higher order input soliton at 2085 nm is fully compressed, no corresponding idler wave is observed because of the short interaction length before the soliton splitting occurs.

In the wavelength range 1.2 μm-2.2 μm, the free-carrier generation is dominated by the two-photon absorption process. Free-carriers are known to modify the propagation dynamics through free-carrier absorption and free-carrier index change. However as the repetition rate of our laser is such that the carrier relaxation time is much shorter than the delay between two pulses, the pump pulse energy is too low for the carrier density to become significant. By taking into account the build-up of free-carriers due to the nonlinear absorption of the 500 μW CW wave, no differences have been observed in the simulations with and without the free-carrier term in Eq. 2. For short pulses ($\approx$ 100 fs) with low energy ($\approx$ 1 pJ) the free-carriers may have an impact on the position of the VM point at GHz-repetition rate.

Finally, as shown by the simulations presented in Fig. 5, replacing the CW probe by a pulsed probe and adjusting its delay with respect to the pump, could lead to a 99.6% frequency conversion efficiency of the probe at 1541 nm into a single idler at 1457 nm. This efficiency is in good agreement with the theoretical efficiency of 99.7% which can be calculated from [42]. Moreover, as previously shown [18], because of the energy conservation, the highly efficient frequency conversion induces a visible spectral change on the soliton pump, a mechanism that has been recognized to be suitable to make useful optical transistors [29, 43]. Therefore, these results proved the ability of nanophotonic waveguides for further demonstrations of integrated all-optical applications.

4. Conclusion

In conclusion, we have experimentally studied an optical analogue of an event horizon in a silicon on insulator nanophotonic waveguide. We have unambiguously observed multiple frequency conversions of a CW wave propagating with an intense pump pulse. These multiple reflections occur after the soliton fission of the input pulse, as demonstrated by the good agreement between the simulations and the experimental results. Because of the absence of soliton self-frequency shift effect in silicon waveguides, the group velocity matched wavelengths corresponding to each lower order solitons generated after the fission remain close to the probe wavelength, a condition that is essential to observe these multiple optical event horizons. The interaction with a single pump pulse is in principle possible by resorting to shorter input pump pulses of the order of 50 fs. Our results constitute the first experimental demonstration of optical analogue of an event horizon in integrated structures where the interaction takes place on short propagation distances and at low power. Moreover, as numerically shown, replacing the input CW probe by a pulsed probe, a quasi complete frequency conversion of the probe as well as a spectral recoil of the pump can be obtained using nanophotonic waveguides at pump energies as low as 200 femtojoule. This very low energy as well as the absence of Raman induced soliton self-frequency shift make silicon nanowires very good candidates to foster further study of potential on-chip efficient frequency converters and all-optical transistors based on the physics of the optical analogue of an event horizon.

Acknowledgments

This work was supported by the Belgian Science Policy Office (BELSPO) Interuniversity Attraction Pole (IAP) project Photonics@be and by the Fonds de la Recherche Fondamentale Collective, Grant No. PDR.T.1084.15.

#253529 Received 6 Nov 2015; revised 19 Dec 2015; accepted 22 Dec 2015; published 5 Jan 2016